Published in final edited form as:
NMR Biomed. 2009 February ; 22(2): 229–239. doi:10.1002/nbm.1312.

Brain temperature and pH measured by ^{1}H chemical shift imaging of a thulium agent

Daniel Coman[||,§,*], **Hubert K. Trubel**[||,*,†,+], **Robert E. Rycyna**[#,⊥], and **Fahmeed Hyder**[||,§,*,‡]

[||]Magnetic Resonance Research Center (MRRC), Yale University, New Haven, CT 06520, USA

[§]Quantitative Neuroscience with Magnetic Resonance (QNMR), Yale University, New Haven, CT 06520, USA

[*]Department of Diagnostic Radiology, Yale University, New Haven, CT 06520, USA

[‡]Biomedical Engineering Yale University, New Haven, CT 06520, USA

[†]University of Witten/Herdecke, Germany

[#]Bruker BioSpin MRI, Billerica, MA 01821, USA

Abstract

Temperature and pH are two of the most important physiological parameters and are believed to be tightly regulated because they are intricately related to energy metabolism in living organisms. Temperature and/or pH data in mammalian brain are scarce, however, mainly due to lack of precise and non-invasive methods. At 11.7T, we demonstrate that a thulium-based macrocyclic complex infused through the blood stream can be used to obtain temperature and pH maps of rat brain *in vivo* by ^{1}H chemical shift imaging (CSI) of the sensor itself in conjunction with a multi-parametric model that depends on several proton resonances of the sensor. Accuracies of temperature and pH determination with the thulium sensor – which has a predominantly extracellular presence – depend on stable signals during the course of the CSI experiment as well as redundancy for temperature and pH sensitivities contained within the observed signals. The thulium-based method compared well with other methods for temperature (^{1}H magnetic resonance spectroscopy (MRS) of N-acetyl aspartate and water; copper-constantan thermocouple wire) and pH (^{31}P MRS of inorganic phosphate and phosphocreatine) assessment, as established by *in vitro* and *in vivo* studies. *In vitro* studies in phantoms with two compartments of differing pH values observed under different ambient temperature conditions generated precise temperature and pH distribution maps. *In vivo* studies in α-chloralose anesthetized and renal-ligated rats revealed temperature (33–34 °C) and pH (7.3–7.4) distributions in the cerebral cortex which are in agreement with observations by other methods. These results demonstrate that the thulium sensor can be used to measure temperature and pH distributions in rat brain *in vivo* simultaneously and accurately with ^{1}H CSI.

Keywords

biosensor; blood flow; energetics; metabolism; paramagnetic; tumor

Address correspondence and reprint requests to: Fahmeed Hyder / Daniel Coman, N135 TAC (MRRC), 300 Cedar Street, Yale University, New Haven, CT 06510, USA, Tel: +1-203-785-6205, Fax: +1-203-785-6643, fahmeed.hyder@yale.edu/daniel.coman@yale.edu.
[+]currently at Bayer HealthCare AG, Wuppertal, Germany
[⊥]currently at Philips Healthcare, Highland Heights, OH 44143-213, USA

Introduction

Both pH and temperature are vital indicators of normal metabolism and physiology in the central nervous system. Usually departure from tightly regulated temperature and pH are considered to be warning signs of life abnormal conditions. Therefore temperature and pH measurements are extremely important for both assessment, and perhaps even treatment, of various pathophysiological states.

In vivo measurements of brain temperature and pH distributions are scarce mainly due to lack of non-invasive methods. Although thermocouple wires provide direct and absolute measure of brain temperature *in vivo* (1), the method is slightly invasive and temperature measurement across wide regions is quite impractical. On the other hand, infrared spectroscopy methods are far less invasive to provide better temperature distributions (2). However optical methods usually provide relative measurements near the dorsal cortical layers. In contrast, magnetic resonance imaging (MRI) and spectroscopy (MRS) allow measurements of both temperature (3) and pH (4) non-invasively using variations of relaxation times, diffusion constants, or chemical shifts of various molecules – both endogenous (e.g., water, N-acetyl aspartate (NAA), inorganic phosphate (Pi), phosphocreatine (PCr)) and exogenous (e.g., shift reagents).

One of the most common MRI methods used for temperature mapping is based on the calculation of water proton resonance frequency using the phase information obtained from gradient echo images (5). Two other water-based MRI methods use dependencies of longitudinal relaxation time (6) or molecular diffusion coefficient (7). With MRS, the water proton resonance frequency in relation to NAA has a temperature sensitivity of 0.01 ppm/°C and is more accurate than both the relaxation time and diffusion methods (8). However further applications of these methods could be pursued if the sensitivities were higher because many other factors (e.g., magnetic susceptibility) can affect the water signal.

The most reliable method for pH uses endogenous ^{31}P intracellular signals of Pi and PCr (9). Recently other ^{31}P methods involving exogenous agents such as 3-aminopropylphosphate have been used in mice (10). ^{1}H MRS provides various options for pH measurements *in vivo* with other exogenous agents. For example, a nontoxic reagent, 2-imidazole-1-yl-3-ethoxycarbonyl-propionic acid, has been used for imaging brain tumors in rodents (11). However these spectroscopic methods for pH determination have relatively low pH sensitivities.

Other ^{1}H MRS methods for pH are based on the chemical exchange saturation transfer or CEST technique (12). The method uses the exchange of hydrogen of either endogenous (amide protons of intracellular proteins and peptides (13)) or exogenous (5,6-dihydrouracil (12) or chelates containing paramagnetic ions called PARACEST agents (14)) molecules. Although the concentration requirement for PARACEST agents is smaller than that of CEST agents, both require determination of ratiometric curves at a given field strength. Recently PARACEST agents have also demonstrated temperature dependence of the hyperfine shift of lanthanide-bound water protons (15). Several ^{19}F MRS methods for pH measurement have been reported. Fluorinated derivatives of vitamin B6 (6-fluoropyridoxol and 6-fluoropyridoxamine) allow the measurement of both intra- and extracellular pH in rodent tumors (16). Another ^{19}F method is based on the extracellular pH dependence of the ZK-150471 probe (17). Although ^{19}F has some advantages over ^{31}P (i.e., high gyromagnetic ratio, large chemical shift dispersion, absence of endogenous ^{19}F resonances), the fluorinated compounds are relatively unstable.

In the last decade, several complexes between lanthanide paramagnetic ions (e.g., thulium, ytterbium) and various macrocyclic chelates – such as 1,4,7,10-tetraazacyclododecane-1,4,7,10-tetrakis(methylene phosphonate) ($DOTP^{8-}$), 1,4,7,10-tetraazacyclododecane-1,4,7,10-tetraacetate ($DOTA^{4-}$), or 1,4,7,10-tetramethyl 1,4,7,10-tetra azacyclodoecane-1,4,7,10-tetraacetic acetate ($DOTMA^{4-}$) – have been proposed as

temperature sensitive probes (18–25). Initially these types of complexes were used as shift reagents (26). As temperature probes they rely on the temperature dependence of their ^{1}H and/or ^{31}P chemical shifts. In general the complexes with the highest temperature sensitivities are the ones containing thulium (Tm^{3+}) as the paramagnetic ion (19). A comparison between the $TmDOTP^{5-}$ and $TmDOTA^{-}$ complexes indicate that all the $TmDOTP^{5-}$ protons have higher temperature sensitivities than the corresponding protons in $TmDOTA^{-}$ (24). The H6 proton of $TmDOTP^{5-}$ has temperature sensitivity of 0.93±0.05 ppm/°C (27) which is higher than that of the corresponding methyl group of $TmDOTMA^{-}$ (~0.57 ppm/°C) (19). Therefore $TmDOTP^{5-}$ represents an excellent temperature sensor. Moreover its proton chemical shifts are also pH dependent, which represents an advantage when trying to measure both temperature and pH. Previously we have shown that $TmDOTP^{5-}$ is present in brain's extracellular space and that temperature and pH can be calculated using two $TmDOTP^{5-}$ proton resonances (27). Here we demonstrate that the majority of the $TmDOTP^{5-}$ signal in a voxel is from extracellular space and that this signal can be successfully used to obtain temperature and pH maps of rat brain. The impact of signal-to-noise ratio (SNR) on chemical shift for accuracy of temperature and pH assessments is compared with other methods.

Materials and Methods

Database for $TmDOTP^{5-}$ (^{1}H MRS)

A database for $TmDOTP^{5-}$ was obtained from various samples containing 3 mM of 3-(Trimethylsilyl)propionic-2,2,3,3-d_4 acid (TSP) and 10% of D_2O with different Ca^{2+} concentrations (0–4 mM) at pH values between 6.9 and 7.7. For each sample, ^{1}H spectra were acquired on an 11.7T Bruker vertical bore spectrometer (Fig. 1) at temperatures between 26 and 40 °C. The spectra were line broadened (50 Hz) and then baseline (first order) and phase (zero order) corrected. The chemical shifts of each $TmDOTP^{5-}$ proton (and water) were measured by fitting to a Lorentzian function. Longitudinal (T_1) and transverse (T_2) relaxation times of the $TmDOTP^{5-}$ protons (Table 1) were measured at 35 °C and pH 7.4 using conventional inversion recovery and spin echo methods. The longest inversion recovery and spin echo times were 5 ms. Single exponential functions were fitted to the data to obtain T_1s and T_2s.

Phantom experiments with $TmDOTP^{5-}$(^{1}H CSI)

The phantom used for *in vitro* experiments consisted of two concentric tubes containing 4 mM $TmDOTP^{5-}$, 3 mM TSP, 10% D_2O, and 1 mM Ca^{2+} but the inner and outer tubes had different pH values (7.0 and 7.4, respectively). 2D CSI data were acquired on a modified 11.7T Bruker horizontal bore spectrometer using a ^{1}H surface coil radio frequency (RF) probe (1.4 cm diameter) using the following parameters: 32×32 or 16×16 encoding steps, dummy scans = 32, repetition time (TR) = 22 ms, number of averages = 16 or 64, field of view = 2.56×2.56 cm, acquisition time = 6 minutes. A 200 μs gaussian excitation pulse was used for selective excitation of a 4 mm slice and the phase encode gradient duration was 100 μs. Two free induction decays (FIDs) were acquired sequentially, one with the transmitter pulse at a frequency between the H2 and H3 protons and the other at the frequency of the H6 proton. These two transmitter frequencies (and the respective bandwidths of the excitations) were determined *a priori* from temperature and pH dependencies of the $TmDOTP^{5-}$ protons within the physiological range (27). The temperature of the phantom was controlled by a water-heating blanket wrapped around the phantom. The ambient temperature inside the bore was measured by a thermocouple wire (~100 μm diameter, copper-constantan; ±0.05 ºC; Oxford Optronix, Oxford, UK) positioned ~5 cm away from the surface coil to avoid any interactions with the thermocouple. No magnetic susceptibility effects of the thermocouple wire were detected in the MRI data. Two different CSI datasets were obtained at two different bath temperatures, 45

and 35 °C, corresponding to respective temperatures of 37.3±0.1 and 30.1±0.1 °C inside the magnet bore as measured by the thermocouple. The spectra were processed as described above.

Temperature and pH by $TmDOTP^{5-}$ (calibration)

An example of the temperature and pH dependencies for the four observable proton resonances of $TmDOTP^{5-}$ is shown in Fig. 2. Because the chemical shifts of these protons do not depend linearly on temperature and/or pH, at least a second order dependence of chemical shift on temperature and/or pH needs could be considered for each proton. The 3D surfaces in Fig. 2 represent the fitted results of chemical shift (δ) as a function of temperature (T) and pH,

$$\delta = A + B \cdot T + C \cdot pH + D \cdot T^2 + E \cdot pH^2 + F \cdot T \cdot pH \quad [1]$$

where A–F are coefficients which were determined analytically. As the temperature increases, all four protons move towards water. For H2 and H3 protons the temperature increase results in a decrease in their chemical shifts, whereas for H6 and H1 protons this results in an increase in their chemical shifts. The pH effect on the chemical shift movement is opposite to the temperature effect. Most importantly, the temperature and pH dependencies of these four protons are different from each other (i.e., each 3D sheet represented in Fig. 2 is unique from the others), providing the possibility to simultaneously determine temperature and pH by exploiting the internal redundancy of the thulium sensor for both physiological parameters (see Results).

Temperature by NAA and water (^{1}H MRS, calibration)

^{1}H spectra of NAA-water were acquired on an 11.7T Bruker horizontal bore spectrometer using a ^{1}H surface RF probe (1.4 cm diameter): voxel size = 6×3×6 mm^3, TR = 2.5 s, number of averages = 384, dummy scans = 4. Samples containing 20 mM NAA, 20 mM phosphate buffer, and 1 mM TSP at pH values of 7.0, 7.2 and 7.4 were studied at temperatures within the range of 20 and 40 °C. Temperature (T) was calculated by

$$T = (309.7 \pm 1.3) + (-102.7 \pm 0.5) \bullet (\delta_{water} - \delta_{NAA}) \quad [2]$$

where δ_{water} and δ_{NAA} represent the water and NAA chemical shifts. The slope and intercept were calculated by linear least-squares regression of water-NAA data for the different conditions described above.

pH by Pi and PCr (^{31}P MRS, calibration)

^{31}P spectra of Pi-PCr were obtained on a 9.4T Bruker horizontal bore spectrometer using a ^{31}P surface coil RF probe (2 cm diameter): voxel size = 7×4×7 mm^3, TR = 2 s, number of averages = 1024, dummy scans = 16. Samples containing 20 mM phosphate and 20 mM phosphocreatine at pH values between 6.6 and 7.7 were used. The pH was calculated by

$$pH = pK_a + \log\left(\frac{\Delta\delta - \delta_1}{\delta_2 - \Delta\delta}\right) \quad [3]$$

where Δδ represents the chemical shift difference between Pi and PCr resonances, δ_1 = 3.23 ppm and δ_2 = 5.70 ppm are the corresponding chemical shift differences at low and high pH, respectively (28), and pK_a = 6.915±0.002 was calculated by linear least-squares regression of Pi-PCr data for the different conditions described above.

Impact of spectral SNR on temperature and pH determination (simulations)

Since the accuracy of temperature/pH calculation by eqs. [1–3] depends on SNR, the effect of SNR on chemical shift determination was assessed by incremental addition of uniformly distributed random noise to the FID. A noise vector, representing a uniform distribution, was constructed with the same length as the complex FID vector. SNR was varied by increasing the noise amplitude. For each noise amplitude value, the modified FID was Fourier transformed and the peak of interest was fitted to a Lorentzian lineshape. No extra line broadening was used, whereas baseline (first order) and phase (zero order) corrections were applied. The SNR for the peak of interest was calculated from "signal" and "noise" measurements (29)

$$\mathrm{SNR}=20\times\log_{10}\left(\frac{\mathrm{signal}}{\mathrm{noise}}\right) \quad [4]$$

where the "signal" was defined as the height of the Lorentzian fitted peak and the "noise" was assessed from the intensity in a specified spectral region containing no resonances (based on *a priori* knowledge). At a designated noise amplitude, an averaged SNR value was obtained from 100 different runs of uniformly distributed random noise. For SNR calculations of $TmDOTP^{5-}$ protons, the temperature and pH were calculated during each of the 100 runs using the model which is an extension of eq. [1] (see Results). Similar procedures were followed for NAA-water (by ^{1}H MRS; eq. [2]) and Pi-PCr (by ^{31}P MRS; eq. [3]) data used for temperature and pH measurements, respectively.

In vivo studies

All animal experimental procedures were approved by the Institutional Animal Care and Use Committee (IACUC). Twelve Sprague-Dawley rats (200–300 g) were tracheotomized and artificially ventilated (70% N_2O, 30% O_2). Halothane (1–2 %) was used for induction and surgery. An intraperitoneal line was inserted for administration of α-chloralose (46±4 mg/kg/hr) and an intravenous line for administration of D-tubocurarine chloride (1 mg/kg/hr) and Na[$TmDOTP^{5-}$] (1 mmol/kg). The rate of $TmDOTP^{5-}$ infusion was adjusted to keep the animal within the autoregulatory range of cerebral perfusion. An arterial line was used for monitoring physiology (blood pH, pO_2, pCO_2) throughout the experiment. The anesthetized rats were prepared with renal ligation as previously described (27). A water-heating blanket was used to control and maintain the body temperature. Eight and four animals were used for MRS and thermocouple measurements, respectively, inside and outside the magnet. The procedures described above were common for both types of experiments. For the thermocouple measurements, a probe (Oxford Optronix Ltd., Oxford, UK) was inserted through a small burr hole to measure cortical temperature (1mm below the dura) continuously (μ1401, CED, Cambridge, UK). To minimize heat exchange with the environment, the head was covered with cotton balls.

The *in vivo* ^{1}H 2D CSI data from rat brain during $TmDOTP^{5-}$ infusion were obtained on a modified 11.7 T Bruker horizontal bore spectrometer using data acquisition parameters for the phantom experiments (see above). The 2D CSI data sets were acquired using 16×16 phase encoding steps and processed similarly as indicated above. *In vivo* temperature and pH were assessed based on *in vitro* calibrations (see Results). The *in vivo* ^{1}H and ^{31}P MRS data of metabolites (containing NAA-water and Pi-PCr, respectively) were acquired using single voxel spectroscopy (see above) to calculate temperature and pH, respectively (eq. [2] and eq. [3]).

The $TmDOTP^{5-}$ concentration *in vivo* (in a CSI voxel) was estimated by comparison with a phantom of known $TmDOTP^{5-}$ concentration, where both data sets were acquired under identical conditions (spatial resolution, acquisition time, data processing, etc.). We used the

H2 and H3 protons for $TmDOTP^{5-}$ concentration estimation. In both cases (i.e., *in vivo* and *in vitro* CSI voxels) the areas under the corresponding resonances were used for quantification. Shimming conditions did not adversely affect this procedure because the $TmDOTP^{5-}$ proton peaks are intrinsically broad due to their extremely short T_2 values (Table 1). This procedure provided the total $TmDOTP^{5-}$ concentration in the CSI voxel (C_t) which contains $TmDOTP^{5-}$ in the blood (C_{bl}) and in the extracellular space (C_{ex}). In a specified cortical region, the blood volume is about 3% (30) and the extracellualar volume is about 20% (31) of the total volume. Since the thulium agent is localized within these two regions, the blood fraction (f_{bl}) contributes by ~13% while the extracellular space fraction (f_{ex}) contributes by ~87% to the total MRS signal. The $TmDOTP^{5-}$ concentration in the extracellular space C_{ex} can be calculated using the total and blood concentrations according to the equation $C_t = f_{bl}\, C_{bl} + f_{ex}\, C_{ex}$. To determine the blood concentration, we removed blood (75–150 μl) from the sagittal sinus after 2 hours from the start of the infusion. The scalp was removed to expose the skull, a small hole was drilled on the sagittal suture, 1 mm above the lambda point and blood was extracted using a capillary glass tube. The blood samples were centrifuged, the supernatant portions were saved, and *ex vivo* samples were made by adding 50 μl of 10 mM TSP in D_2O and distilled water to bring the final volume to 500 μl. ^1H spectra were acquired on the 11.7T Bruker vertical bore spectrometer (see above).

Results

In vitro measurements

Two of the six non-exchangeable and non-equivalent protons of $TmDOTP^{5-}$ (Fig. 1), H4 and H5, have resonances at approximately +500 ppm and −385 ppm, respectively, from the water resonance. Therefore simultaneous detection of all six protons requires an extremely large spectral bandwidth (~1000 ppm). The smaller intensities of these two resonances are due to limited excitation over the far ends of the excited bandwidth. Thus the spectral bandwidth needs to be restricted to a smaller range (~300 ppm) to acquire signals with reasonable SNR – namely the H1, H2, H3 and H6 resonances.

The presence of a paramagnetic ion (Tm^{3+}) inside the $DOTP^{8-}$ macrocyclic complex enhances T_1 and T_2 relaxation of the protons, most likely dominated by dipolar relaxation between the unpaired Tm^{3+} electron and the proton nuclear spin. Previous results at 7T suggest relaxation times on the order of several milliseconds (25). Such short relaxation times restrict the design of complex ^1H MRS pulse sequences (e.g., involving outer volume suppression or water suppression). Our 11.7T measurements at 35 °C (Table 1) indicate that, out of the four protons investigated, the H6 has the longest T_1 and T_2 relaxation times (1.6±0.1 ms and 0.73±0.06 ms, respectively). The extremely short T_2 values (less than 0.73 ms) drastically restrict the TR of the MRS pulse sequence (i.e., elapsed time between excitation and acquisition) to less than 1 ms. Under these conditions the most suitable method to obtain localized detection of $TmDOTP^{5-}$ signals is 2D CSI. Water suppression was not required given the use of a frequency selective gaussian pulse and the fact that the $TmDOTP^{5-}$ proton frequencies are at least 20 MHz away from the water frequency.

Temperature and pH calibration for $TmDOTP^{5-}$

The different dependencies of $TmDOTP^{5-}$ proton chemical shifts on temperature and pH (Fig. 2) can allow simultaneous prediction of these vital parameters. Our previous results showed that temperature and pH can be calculated simultaneously using chemical shifts of two different $TmDOTP^{5-}$ protons (27). However this method did not fully account for presence of Ca^{2+} interactions with $TmDOTP^{5-}$ *in vivo*. In rat brain, Ca^{2+} concentration in interstitial fluid is ~1 mM (32–34). Since previous results indicate that Ca^{2+} forms a stable adduct with

$TmDOTP^{5-}$ (35), the *in vitro* calibration for temperature and pH should consider the involvement of Ca^{2+} and $TmDOTP^{5-}$ interactions.

Given that the *in vivo* $TmDOTP^{5-}$ concentrations measured in a CSI voxel and sagittal sinus were 4.0±0.1 mM and 5.7±0.3 mM respectively, the $TmDOTP^{5-}$ concentration in the extracellular space was calculated to be 3.75±0.12 mM (Table 2). Therefore the *in vitro* calibrations were carried out with spectra from the database containing a range of Ca^{2+} and $TmDOTP^{5-}$ concentrations (see above) to match the *in vivo* Ca^{2+}:Tm^{3+} ratio of about 1:4. In addition, our results suggest that about 82% of the *in vivo* $TmDOTP^{5-}$ signal in a CSI voxel is of non-blood origin and therefore the temperature and pH calculated using the $TmDOTP^{5-}$ method would be sensitive to the extracellular compartment.

The current multi-parametric model exploits the redundant temperature and pH information contained in the chemical shifts of $TmDOTP^{5-}$ protons. Since the H1 proton has an extremely short T_2 (0.32±0.03 ms), the peak is very broad and under *in vivo* conditions this proton has a much lower SNR than the other three protons. Therefore the model is based on the chemical shifts of the H2, H3, and H6 protons. To find the combination of protons that produce the smallest error in temperature and pH determination, several scenarios were considered. For the model using two protons (x and y), the temperature ($T_c^{[x,y]}$) and pH ($pH_c^{[x,y]}$) were calculated from their respective chemical shifts (δ_x and δ_y) according to

$$T_c^{[x,y]}=a_1^{[x,y]}+a_2^{[x,y]}\delta_x+a_3^{[x,y]}\delta_y+a_4^{[x,y]}\delta_x{}^2+a_5^{[x,y]}\delta_y{}^2+a_6^{[x,y]}\delta_x\delta_y \quad [5]$$

$$pH_c^{[x,y]}=b_1^{[x,y]}+b_2^{[x,y]}\delta_x+b_3^{[x,y]}\delta_y+b_4^{[x,y]}\delta_x{}^2+b_5^{[x,y]}\delta_y{}^2+b_6^{[x,y]}\delta_x\delta_y \quad [6]$$

Where the coefficients $a_i^{[x,y]}$ and $b_i^{[x,y]}$ (i=1 to 6) were calculated from the linear least-squares fits of temperature and pH, respectively, as function of chemical shifts (Table 3 and Table 4). For the model using all three protons, the temperature and pH were calculated in two ways. First, averaged temperature and pH values were obtained from three combinations of two protons: [H2,H6], [H3,H6] and [H2,H3]. Second, averaged temperature and pH values were obtained from two combinations of two protons: [H2,H6] and [H3,H6], [H2,H6] and [H2,H3], [H3,H6] and [H2,H3]. Assuming the same error in the chemical shift measurement for all protons (ε_δ) and with propagation of errors (36) it can be shown that the uncertainties in temperature (ε_T) and pH (ε_{pH}) are both proportional to the error in the chemical shift measurement. Our results indicated that the smallest error in both temperature and pH determination was obtained with the model based on two combinations of two protons, namely [H2,H6] and [H3,H6]. In this case, at 35 °C and pH of 7.4, we estimated that the errors in temperature and pH were $\varepsilon_T = 2.63 \bullet \varepsilon_\delta$ and $\varepsilon_{pH} = 0.482 \bullet \varepsilon_\delta$, respectively. Based on this error analysis, the most reliable way to calculate temperature ($T_c^\bullet$) and pH ($pH_c^\bullet$) from H2, H3 and H6 resonances is by using

$$T_c^\bullet=(T_c^{[H2,H6]}+T_c^{[H3,H6]})/2 \quad [7]$$

$$pH_c^\bullet=(pH_c^{[H2,H6]}+pH_c^{[H3,H6]})/2 \quad [8]$$

where $T_c^{[H2,H6]}$, $T_c^{[H3,H6]}$, $pH_c^{[H2,H6]}$ and $pH_c^{[H3,H6]}$ are given by eq. [5] and eq. [6]. The comparison between calculated ($T_c^\bullet$) and measured (T_m) temperatures gave

$$T_c^{\bullet} = (0.016 \pm 0.075) + (0.999 \pm 0.002) \bullet T_m \quad [9]$$

with a high correlation coefficient (R = 0.99978) as obtained by linear least-squares fit. A similarly good correlation (R = 0.99654) was found between calculated ($pH_c^{\bullet}$) and measured (pH_m) pH.

$$pH_c^{\bullet} = (0.058 \pm 0.064) + (0.992 \pm 0.009) \bullet pH_m \quad [10]$$

For both temperature and pH, the correlation between calculated and measured values was ~1 with an intercept of ~0 indicating excellent accuracy. Using the *in vitro* calibration at 1 mM Ca^{2+} and 4 mM $TmDOTP^{5-}$, we calculated temperature sensitivities of $TmDOTP^{5-}$ protons at 35 °C and pH of 7.4 to be 1.27, −0.59, −0.46 and 1.00 ppm/°C for H1, H2, H3 and H6 protons, respectively. The corresponding pH sensitivities were −4.23, 4.16, 3.61 and −3.91 ppm/pH units for H1, H2, H3 and H6 protons, respectively. This calibration holds for the wide range of temperature (26 to 40 °C) and pH (6.9 to 7.7) expected *in vivo*.

Effect of spectral SNR on temperature and pH determination

The error in temperature and pH determination depends on the error in chemical shift measurement, which in turn depends on the SNR for each proton resonance. Simulation results with $TmDOTP^{5-}$ show that the standard deviation in the chemical shift for H1 proton is larger than for the H2, H3 and H6 protons at the same SNR value. The temperature and pH values were calculated with variable SNR values from the chemical shifts of H2, H3 and H6 (eq. [5] to eq. [8]) and the standard deviations for temperature and pH estimations were obtained (Figs. 3A and 3B, respectively). Typical *in vivo* SNR values for H2, H3 and H6 protons in a 2D CSI voxel (of a 1.6×1.6×4 mm^3) is ~15 with total acquisition time of 6 minutes. At this SNR the standard deviations of temperature and pH were 0.008 °C (Fig. 3A) and 0.0013 (Fig. 3B), respectively.

Similarly the standard deviations in temperature and pH using the NAA-water and Pi-PCr methods, respectively, were estimated for a range of SNR values (Figs. 3C and 3D). Under similar conditions (i.e., in terms of voxel size and total acquisition time of a 2D CSI experiment for $TmDOTP^{5-}$), the SNR values for the methyl NAA group and Pi-PCr were ~8 and ~5, respectively. These SNR values for NAA-water and Pi-PCr methods corresponded to standard deviations of 0.06 °C for temperature and 0.004 for pH, respectively. The comparison of results from the different methods shows that the standard deviations in temperature and pH measured by the $TmDOTP^{5-}$ method are at least as good as in the other methods, thereby suggesting that both temperature and pH can be measured rapidly and simultaneously using 2D CSI of $TmDOTP^{5-}$. However both NAA-water and Pi-PCr methods reflect predominantly intracellular events, whereas the $TmDOTP^{5-}$ method reflects mostly extracellular events.

Phantom measurements of temperature and pH

A phantom with two different pH values in each of its two compartments (inner at 7.0 and outer at 7.4) was used to demonstrate the feasibility of generating high resolution temperature and pH maps with $TmDOTP^{5-}$, where the magnet bore temperature was varied by ~7 °C (Fig. 4). Rapidly acquired high resolution 2D CSI data provided well resolved spectra of the entire phantom (Fig. 4A). Chosen voxels from the outer and inner compartments (Fig. 4B, upper and lower spectra, respectively) revealed that the chemical shifts move towards the water resonance as the pH decreases, as expected from the temperature and pH dependencies of $TmDOTP^{5-}$ (Fig. 2). Using the H2, H3 and H6 protons, the temperature and pH values were calculated for each voxel according to the model described above. Temperature and pH maps were generated

for two different ambient temperature conditions, one corresponding to a bore temperature of 37.3±0.1 °C (Fig. 4C) and another to 30.1±0.1 °C (Fig. 4D). For the first case (Fig. 4C), the results indicated that the average calculated temperatures in the outer and inner compartments were 37.2±0.3 °C and 37.0±0.3 °C, respectively, with average calculated pH values of 7.39 ±0.05 and 7.01±0.05. These results are in excellent agreement with the measured values of temperature (37.3±0.1 °C) and pH (7.4±0.1 and 7.0±0.1, respectively, in the two compartments). Similar agreements were found when the bore temperature was lowered (Fig. 4D). The average calculated temperatures in the outer and inner compartments were 30.0±0.3 °C and 29.9±0.3 °C, respectively, with average calculated pH values of 7.40±0.06 and 7.05 ±0.07. When voxels sizes of the CSI experiment in this phantom were increased (i.e., SNR was raised), the agreement between calculated and measured values improved slightly (data not shown), which agrees with the conclusions from the SNR-based simulations (Fig. 3).

Brain temperature and pH maps

$TmDOTP^{5-}$ concentration in the blood and in the extracellular spaces became quite stable within 2 hours of infusion (Table 2). Repeated measurements over several hours did not change significantly from these steady-state values, probably because renal ligation drastically diminished the amount of $TmDOTP^{5-}$ lost over time. All CSI experiments were acquired during the stable period to ensure that the *in vivo* conditions were similar to those used for temperature and pH calibration (i.e., Ca^{2+}:$TmDOTP^{5-}$ ratio of 1:4). *In vivo* detection of $TmDOTP^{5-}$ with high SNR (Fig. 5A) shows well resolved H2, H3 and H6 resonances in 10 μl voxels (Fig. 5B). The temperature (Fig. 5C) and pH (Fig. 5D) maps of rat brain show that the average cortical values were 34.3 °C and 7.40, respectively. The temperature in the upper cortical regions was between 33.7 and 34.2 °C and slightly higher ranges were found in deeper cortical regions (between 34.3 to 34.9 °C). Likewise the pH distribution was relatively uniform, with values ranging between 7.29 and 7.41 in upper cortical regions. The core body temperature was 35.8±0.1 °C, where the standard deviation of 0.1 °C represents the fluctuations of the body temperature during the acquisition period. Measurements with thermocouple wires in a separate group (n = 4) but under the same conditions indicated that the average temperatures in the cortex (1 mm below dura) and basal ganglia (4 mm below dura) were 35.4±0.8 and 37.2 ±0.7 °C, respectively, where the corresponding standard deviations indicate the variations about the mean for four animals investigated. Moreover the cortical temperature measured by the NAA-water method and pH using ^{31}P MRS in slightly larger voxels (data not shown, under similar conditions) were 35.2±0.4 °C and 7.30±0.01, respectively. These independent temperature and pH values are in excellent agreement with the $TmDOTP^{5-}$ results.

Discussion

The method presented here demonstrates that two important parameters which are commonly used to discern various metabolic processes *in vivo*, temperature and pH, can be simultaneously measured using three proton chemical shifts of $TmDOTP^{5-}$ (Fig. 1). Because the temperature and pH information is “stored” differentially and independently in each of the chemical shifts of these three protons (Fig. 2), their redundant dependencies can be used to increase the accuracies of temperature and pH predictions (Table 3 and Table 4). While the simultaneous dependence of chemical shifts on both temperature and pH can be seen as a drawback for accurate determination of these two parameters, we propose that simultaneous measurement of temperature and pH from $TmDOTP^{5-}$ protons can instead be an experimental asset since the acid-base balance is inherently linked to temperature in most tissues (37). Thus with one exogenous agent both vital parameters can be measured by biosensor imaging of redundant deviation of shifts (BIRDS).

The error in temperature and pH calculation from any MRS measurement is dependent on spectral SNR through the error in chemical shift determination. Our simulations indicate that for typical *in vivo* SNR range with $TmDOTP^{5-}$ (10 to 30) the range of errors for temperature and pH predictions are better than 0.02 °C and 0.003, respectively (Figs. 3A and 3B). Under similar *in vivo* conditions, the errors for temperature and pH measured by NAA-water and Pi-PCr methods, respectively, are quite similar (Figs. 3C and 3D). It should be noted, however, that the simulations for NAA-water and Pi-PCr methods did not take into account the additional confounds of spectral overlap between the assigned and other metabolites. For example, the *in vivo* NAA methyl group resonance at 2.01 ppm overlaps with a resonance from N-acetyl aspartatyl glutamate at 2.04 ppm and another resonance from glutamate at 2.05 ppm (28), thereby inducing deviations from Lorentzian lineshapes. In contrast, for the $TmDOTP^{5-}$ method all proton resonances are well resolved and there are no concerns about spectral overlap with other resonances. However an important distinction between these MRS methods is that the NAA-water and Pi-PCr methods do not require infusion of an exogenous agent and no renal ligation is needed. However the extremely short T_1 and T_2 relaxation times of $TmDOTP^{5-}$ protons, on the order of milliseconds, have two opposite effects on the corresponding SNR. A short T_2 produces a large linewidth to thereby decrease SNR, while a short T_1 allows for faster averaging which in turn increases the SNR. Fast averaging is extremely important for obtaining temperature and pH distributions in real time during various applications.

Our *in vitro* results showed that high resolution temperature and pH maps can be obtained using the BIRDS method using $TmDOTP^{5-}$ (Fig. 4). Excellent agreement was observed between the bore temperatures and the average calculated temperatures in the two compartments. Also the calculated pH distributions showed excellent agreement with the measured pH values in the two compartments for two different bore temperatures. The similarity between the pH distributions in the two compartments (at both bore temperatures) demonstrates that the temperature determination is indeed independent of pH, and therefore this calibration may be applied *in vivo*. Although the *in vivo* toxicity of $TmDOTP^{5-}$ has not been measured directly, it can be inferred from other observations. Results in our (27) and other (38) laboratories suggest that infusion dose of 1 mmol/kg results in stable systemic physiology without affecting normal brain function (HKT and FH unpublished results). Moreover the half lethal dose (LD_{50}) values for lanthanide complexes such as $YbDOTMA^-$ (18) or $GdDOTA^-$ (39) are 10.5 mmol/kg and 11.4 mmol/kg, respectively, suggesting that the LD_{50} for $TmDOTP^{5-}$ may be at least an order of magnitude higher than the doses used in our experiments.

It has been suggested (22,40) that $TmDOTP^{5-}$ or other similar compounds (e.g., $TmDOTMA^-$) do not cross the blood-brain barrier. Our previous (27) and current results suggest that $TmDOTP^{5-}$ crosses the blood-brain barrier quite rapidly (1 hour). A plausible delivery route for $TmDOTP^{5-}$ into the extracellular space may be through fenestrated blood vessels. Early in brain development, the endothelium of fenestrated vessels has small apertures which allow various solutes to cross into the extracellular space. However by fetal day 17, these fenestrated vessels disappear from the brain parenchyma (41) except for the circumventricular organs (42). We propose that fenestrated vessels of the circumventricular organs (43) may provide the path for delivery of agents like $TmDOTP^{5-}$ or $TmDOTMA^-$ (and perhaps even other similar agents). The observation of proton signals emanating from the $TmDOTP^{5-}$ complex is drastically enhanced by renal ligation which minimizes its clearance from the body. The present measurements suggest that the *in vivo* $TmDOTP^{5-}$ concentration in a CSI voxel in rat brain is 4.0±0.1 mM after about 2 hours of infusion, while the $TmDOTP^{5-}$ concentration in the sagittal sinus is 5.7±0.3 mM. Based on these results we calculated that the concentration of $TmDOTP^{5-}$ in the extracellular milieu is 3.75±0.12 mM, which represents about 82% of the total signal in a CSI voxel. Because of continuous fast exchange of water (and other molecules) between the inside and outside of the cell, it is possible

that the extracellular temperature measured by the $TmDOTP^{5-}$ method represents a good approximation of the intracellular situations measured by the NAA-water method (see Results).

In vivo results demonstrated that temperature and pH maps of rat brain can be obtained by conventional CSI requiring at most a few minutes to image the $TmDOTP^{5-}$ complex (Fig. 5). The voxels situated at the brain surface had temperature values between 33 and 34 °C, while temperature values in deeper cortical regions were in the range of 34 to 35 °C (Fig. 5C). The results indicated that the anesthetized brain temperature (33–35 °C) can be slightly lower than the body temperature (~36 °C) (44). These results are in good agreement with a recent study in rats (45) which shows that the brain temperature is lower than the body temperature and that deeper brain regions have higher temperature values than the superficial regions. The pH distribution in the cortex shows relative homogeneity between 7.3 and 7.4 (Fig. 5D). While the results in Fig. 5 are from one rat, similar data were obtained from all eight rats scanned.

The temperature and pH measurements from the BIRDS method using $TmDOTP^{5-}$ are in good agreement with independent methods used for each of these physiological parameters (see Results). There is, however, a relatively small effect of Ca^{2+} ions on the chemical shift of the $TmDOTP^{5-}$ protons. Although the calibration depends slightly on the Ca^{2+}:$TmDOTP^{5-}$ ratio, the CSI experiments were acquired after 2 hours of $TmDOTP^{5-}$ infusion when the concentrations in the blood and in the extracellular space were stable (Table 2). Under these conditions, the $TmDOTP^{5-}$ concentration in the extracellular space was 3.75±0.12 mM. Given that Ca^{2+} in the extracellular space is ~1 mM (32–34) and the largest physiological variations in the extracellular space are in the nM range, the *in vivo* Ca^{2+}:$TmDOTP^{5-}$ ratio is within 5–7% of the *in vitro* calibration values. This systematic error corresponds to chemical shift changes of −0.035 ppm, −0.032 ppm, and 0.022 ppm for H2, H3, and H6 resonances, respectively. Therefore slight experimental variations of the Ca^{2+}:$TmDOTP^{5-}$ ratio *in vivo* could correspond to additional temperature and pH errors of 0.025 °C and 0.012, respectively. In total, the estimated error in temperature and pH prediction by the $TmDOTP^{5-}$ method would be on the order of 0.04 °C and 0.015, respectively, which is within the margin of error of the other methods.

In a recent study in α-chloralose anesthetized rats, temperature dynamics in the brain during forepaw stimulation were measured with thermocouples (46). The model considered four simultaneous processes that contributed to temperature changes in a local region: metabolic heat production, removal/addition of heat through blood flow, conductive heat loss to adjacent regions in the brain, and dissipative heat loss to the environment from the brain. A similar approach can be used to model temperature dynamics in the rat brain using temperature distributions obtained using the $TmDOTP^{5-}$ complex. The advantage of the CSI method based on $TmDOTP^{5-}$ in such a study would be that it can be used to map temperature dynamics of the whole brain rather than just a local region.

In summary, in the present study we described a model which uses the redundant chemical shift information from three protons of $TmDOTP^{5-}$ to generate independent and simultaneous temperature and pH distributions. Our results indicated that the BIRDS method using $TmDOTP^{5-}$ compared well with other methods. Simultaneous temperature and pH maps of rat brain were obtained within several minutes using the BIRDS method. The present results open the way towards obtaining simultaneous temperature and pH distributions in a large variety of applications, such as functional activation (47), brain cooling (48) or cancer treatment (49).

Acknowledgements

Thanks to Drs. Basavaraju G. Sanganahalli and Peter Herman for consultations. We thank Peter Brown and Bei Wang for engineering and surgical help. Supported by National Institutes of Health grants (R01 MH-067528, R01 DC-003710, P30 NS-52519).

References

1. Young CC, Sladen RN. Temperature monitoring. Int Anesthesiol Clin 1996;34(3):149–174. [PubMed: 8894753]
2. Brugge JF, Poon PW, So AT, Wu BM, Chan FH, Lam FK. Thermal images of somatic sensory cortex obtained through the skull of rat and gerbil. Exp Brain Res 1995;106(1):7–18. [PubMed: 8542979]
3. Denis de Senneville B, Quesson B, Moonen CT. Magnetic resonance temperature imaging. Int J Hyperthermia 2005;21(6):515–531. [PubMed: 16147437]
4. Gillies RJ, Raghunand N, Garcia-Martin ML, Gatenby RA. pH imaging. A review of pH measurement methods and applications in cancers. IEEE Eng Med Biol Mag 2004;23(5):57–64. [PubMed: 15565800]
5. De Poorter J, De Wagter C, De Deene Y, Thomsen C, Stahlberg F, Achten E. Noninvasive MRI thermometry with the proton resonance frequency (PRF) method: in vivo results in human muscle. Magn Reson Med 1995;33(1):74–81. [PubMed: 7891538]
6. Parker DL, Smith V, Sheldon P, Crooks LE, Fussell L. Temperature distribution measurements in two-dimensional NMR imaging. Med Phys 1983;10(3):321–325. [PubMed: 6877179]
7. Le Bihan D, Delannoy J, Levin RL. Temperature mapping with MR imaging of molecular diffusion: application to hyperthermia. Radiology 1989;171(3):853–857. [PubMed: 2717764]
8. Wlodarczyk W, Boroschewski R, Hentschel M, Wust P, Monich G, Felix R. Three-dimensional monitoring of small temperature changes for therapeutic hyperthermia using MR. J Magn Reson Imaging 1998;8(1):165–174. [PubMed: 9500276]
9. Petroff OA, Prichard JW, Behar KL, Alger JR, Shulman RG. In vivo phosphorus nuclear magnetic resonance spectroscopy in status epilepticus. Ann Neurol 1984;16(2):169–177. [PubMed: 6476792]
10. Gillies RJ, Liu Z, Bhujwalla Z. 31P-MRS measurements of extracellular pH of tumors using 3-aminopropylphosphonate. Am J Physiol 1994;267(1 Pt 1):C195–C203. [PubMed: 8048479]
11. Garcia-Martin ML, Herigault G, Remy C, et al. Mapping extracellular pH in rat brain gliomas in vivo by 1H magnetic resonance spectroscopic imaging: comparison with maps of metabolites. Cancer Res 2001;61(17):6524–6531. [PubMed: 11522650]
12. Ward KM, Balaban RS. Determination of pH using water protons and chemical exchange dependent saturation transfer (CEST). Magn Reson Med 2000;44(5):799–802. [PubMed: 11064415]
13. Zhou J, Payen JF, Wilson DA, Traystman RJ, van Zijl PC. Using the amide proton signals of intracellular proteins and peptides to detect pH effects in MRI. Nat Med 2003;9(8):1085–1090. [PubMed: 12872167]
14. Zhang S, Merritt M, Woessner DE, Lenkinski RE, Sherry AD. PARACEST agents: modulating MRI contrast via water proton exchange. Acc Chem Res 2003;36(10):783–790. [PubMed: 14567712]
15. Zhang S, Malloy CR, Sherry AD. MRI thermometry based on PARACEST agents. J Am Chem Soc 2005;127(50):17572–17573. [PubMed: 16351064]
16. Mason RP. Transmembrane pH gradients in vivo: measurements using fluorinated vitamin B6 derivatives. Curr Med Chem 1999;6(6):481–499. [PubMed: 10213795]
17. Ojugo AS, McSheehy PM, McIntyre DJ, et al. Measurement of the extracellular pH of solid tumours in mice by magnetic resonance spectroscopy: a comparison of exogenous (19)F and (31)P probes. NMR Biomed 1999;12(8):495–504. [PubMed: 10668042]
18. Aime S, Botta M, Fasano M, et al. A new ytterbium chelate as contrast agent in chemical shift imaging and temperature sensitive probe for MR spectroscopy. Magn Reson Med 1996;35(5):648–651. [PubMed: 8722814]
19. Hekmatyar SK, Hopewell P, Pakin SK, Babsky A, Bansal N. Noninvasive MR thermometry using paramagnetic lanthanide complexes of 1,4,7,10-tetraazacyclodoecane-alpha,alpha',alpha'',alpha'''-

tetramethyl-1, 4,7,10-tetraacetic acid (DOTMA4-). Magn Reson Med 2005;53(2):294–303. [PubMed: 15678553]

20. Hekmatyar SK, Kerkhoff RM, Pakin SK, Hopewell P, Bansal N. Noninvasive thermometry using hyperfine-shifted MR signals from paramagnetic lanthanide complexes. Int J Hyperthermia 2005;21 (6):561–574. [PubMed: 16147440]
21. Hekmatyar SK, Poptani H, Babsky A, Leeper DB, Bansal N. Non-invasive magnetic resonance thermometry using thulium-1,4,7,10-tetraazacyclododecane-1,4,7,10-tetraacetate (TmDOTA(−)). Int J Hyperthermia 2002;18(3):165–179. [PubMed: 12028635]
22. Pakin SK, Hekmatyar SK, Hopewell P, Babsky A, Bansal N. Non-invasive temperature imaging with thulium 1,4,7,10-tetraazacyclododecane-1,4,7,10-tetramethyl-1,4,7,10-tetraacetic acid (TmDOTMA-). NMR Biomed 2006;19(1):116–124. [PubMed: 16404728]
23. Zuo CS, Bowers JL, Metz KR, Nosaka T, Sherry AD, Clouse ME. TmDOTP5-: a substance for NMR temperature measurements in vivo. Magn Reson Med 1996;36(6):955–959. [PubMed: 8946362]
24. Zuo CS, Mahmood A, Sherry AD. TmDOTA-: a sensitive probe for MR thermometry in vivo. J Magn Reson 2001;151(1):101–106. [PubMed: 11444943]
25. Zuo CS, Metz KR, Sun Y, Sherry AD. NMR temperature measurements using a paramagnetic lanthanide complex. J Magn Reson 1998;133(1):53–60. [PubMed: 9654468]
26. Buster DC, Castro MM, Geraldes CF, Malloy CR, Sherry AD, Siemers TC. Tm(DOTP)5-: a 23Na+ shift agent for perfused rat hearts. Magn Reson Med 1990;15(1):25–32. [PubMed: 2374497]
27. Trubel HK, Maciejewski PK, Farber JH, Hyder F. Brain temperature measured by 1H-NMR in conjunction with a lanthanide complex. J Appl Physiol 2003;94(4):1641–1649. [PubMed: 12626478]
28. de Graaf, RA. Vol. 2nd Edition. Chichester, West Sussex, England: Wiley, John & Sons, Incorporated; 2007. *In vivo* NMR Spectroscopy - Principles and Techniques.
29. Morton DW, Maravilla KR, Meno JR, Winn HR. Clinically relevant rat model for testing BOLD functional MR imaging techniques by using single-shot echo-planar imaging at 1.5 T. Radiology 2001;218(2):598–601. [PubMed: 11161185]
30. Bereczki D, Wei L, Otsuka T, et al. Hypercapnia slightly raises blood volume and sizably elevates flow velocity in brain microvessels. Am J Physiol 1993;264(5 Pt 2):H1360–H1361. [PubMed: 8498549]
31. Korf J, Postema F. Rapid shrinkage of rat striatal extracellular space after local kainate application and ischemia as recorded by impedance. J Neurosci Res 1988;19(4):504–510. [PubMed: 3385805]
32. Jones HC, Keep RF. Brain fluid calcium concentration and response to acute hypercalcaemia during development in the rat. J Physiol 1988;402:579–593. [PubMed: 3236250]
33. Somjen GG. Ion regulation in the brain: implications for pathophysiology. Neuroscientist 2002;8(3): 254–267. [PubMed: 12061505]
34. Somjen GG, Allen BW, Balestrino M, Aitken PG. Pathophysiology of pH and Ca2+ in bloodstream and brain. Can J Physiol Pharmacol 1987;65(5):1078–1085. [PubMed: 3113705]
35. Ren J, Sherry AD. ^{7}Li, ^{6}Li, ^{23}Na, ^{133}Cs Multinuclear NMR Studies of Adducts Formed with the Shift Reagent, TmDOTP^{5-}. Inorg Chim Acta 1996;246:1–11.
36. Bevington, PR. New York, NY: McGraw-Hill Book Company; 1969. Data Reduction and Error Analysis for The Physical Sciences; p. 336
37. Boron WF. Regulation of intracellular pH. Adv Physiol Educ 2004;28(1–4):160–179. [PubMed: 15545345]
38. Winter PM, Bansal N. TmDOTP^{5-} as a ^{23}Na shift reagent for the subcutaneously implanted 9L gliosarcoma in rats. Magn Reson Med 2001;45(3):436–442. [PubMed: 11241701]
39. Bousquet JC, Saini S, Stark DD, et al. Gd-DOTA: characterization of a new paramagnetic complex. Radiology 1988;166(3):693–698. [PubMed: 3340763]
40. Bansal N, Germann MJ, Lazar I, Malloy CR, Sherry AD. In vivo Na-23 MR imaging and spectroscopy of rat brain during TmDOTP5- infusion. J Magn Reson Imaging 1992;2(4):385–391. [PubMed: 1633390]
41. Yoshida Y, Yamada M, Wakabayashi K, Ikuta F. Endothelial fenestrae in the rat fetal cerebrum. Brain Res Dev Brain Res 1988;44(2):211–219.

42. Brightman MW. The intracerebral movement of proteins injected into blood and cerebrospinal fluid of mice. Prog Brain Res 1968;29:19–40. [PubMed: 4898331]
43. Johnson AK, Gross PM. Sensory circumventricular organs and brain homeostatic pathways. Faseb J 1993;7(8):678–686. [PubMed: 8500693]
44. Kiyatkin EA. Brain temperature fluctuations during physiological and pathological conditions. Eur J Appl Physiol 2007;101(1):3–17. [PubMed: 17429680]
45. Zhu M, Ackerman JJ, Sukstanskii AL, Yablonskiy DA. How the body controls brain temperature: the temperature shielding effect of cerebral blood flow. J Appl Physiol 2006;101(5):1481–1488. [PubMed: 16840581]
46. Trubel HK, Sacolick LI, Hyder F. Regional temperature changes in the brain during somatosensory stimulation. J Cereb Blood Flow Metab 2006;26(1):68–78. [PubMed: 15959461]
47. Maandag NJ, Coman D, Sanganahalli BG, et al. Energetics of neuronal signaling and fMRI activity. Proc Natl Acad Sci U S A 2007;104(51):20546–20551. [PubMed: 18079290]
48. Trubel H, Herman P, Kampmann C, et al. A novel approach for selective brain cooling: implications for hypercapnia and seizure activity. Intensive Care Med 2004;30(9):1829–1833. [PubMed: 15185071]
49. van der Zee J. Heating the patient: a promising approach? Ann Oncol 2002;13(8):1173–1184. [PubMed: 12181239]

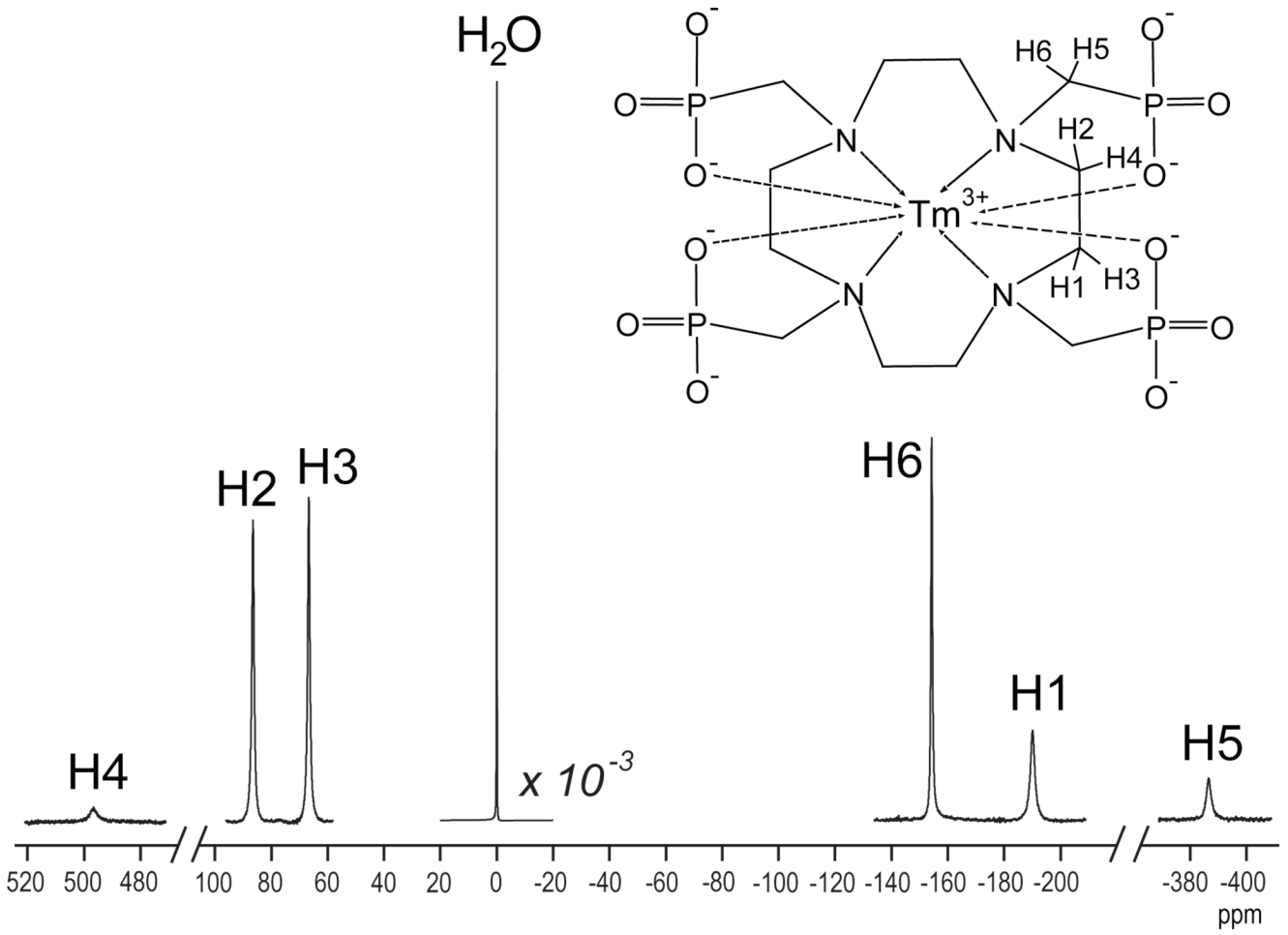

Figure 1.

^{1}H spectrum at 11.7T (500 MHz) of a sample containing 10 mM $TmDOTP^{5-}$. The water signal (at 0 ppm) was decreased by three orders of magnitude, while for all the other resonances the vertical scale was the same. Assignment of the six non-exchangeable and non-equivalent proton resonances from the macrocyclic chelate are also shown.

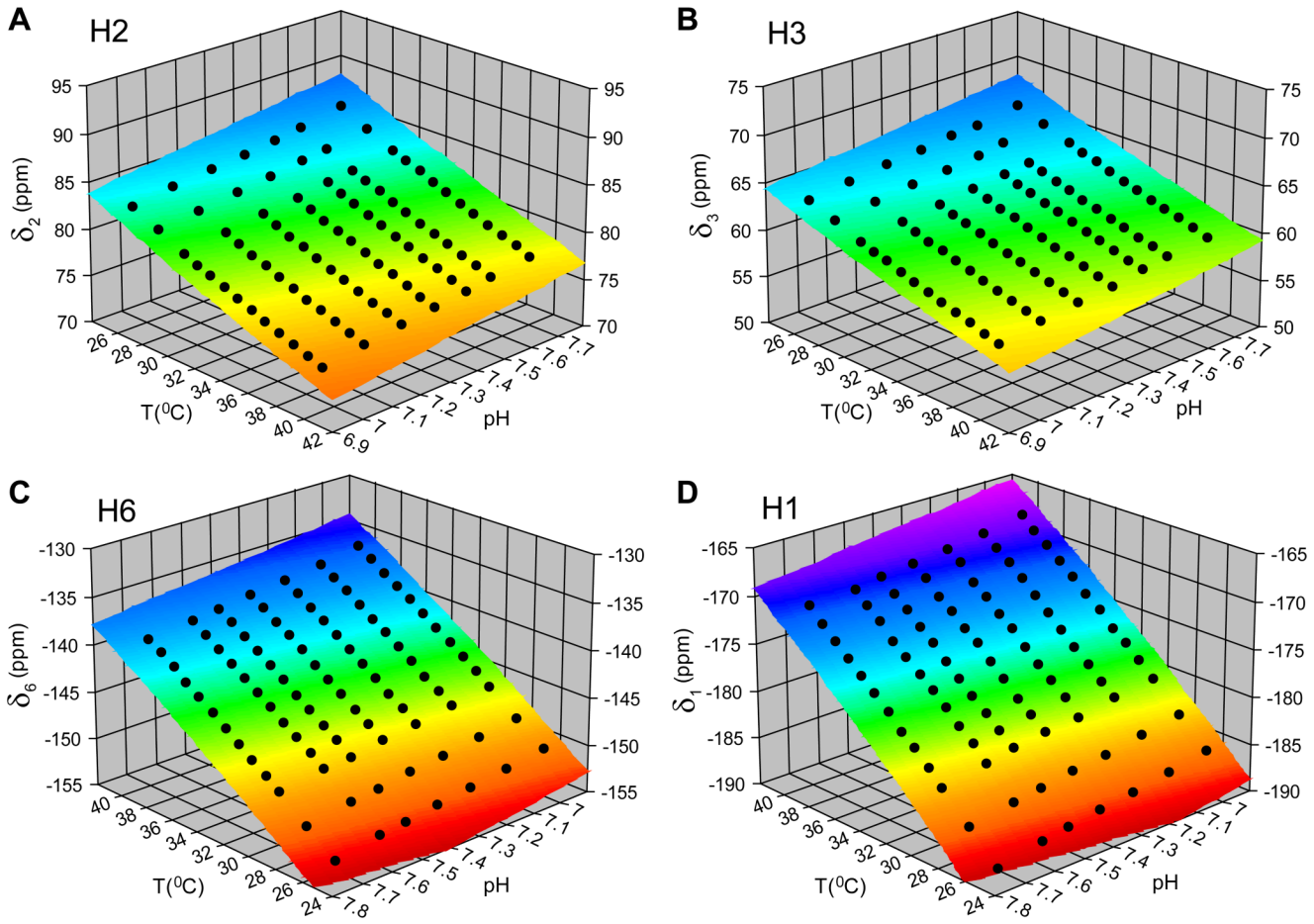

Figure 2.

Temperature and pH dependencies of H2, H3 H6 and H1 proton chemical shifts (δ_2, δ_3, δ_6 and δ_1) of $TmDOTP^{5-}$ are shown in (A), (B), (C) and (D), respectively, for an *in vitro* sample (4 mM $TmDOTP^{5-}$, 1 mM Ca^{2+}, 10% D_2O). The 3D surfaces represent the result of the fits of chemical shift δ as function of temperature T and pH (eq. [1]). The differential and independent "storage" of temperature and pH information by each of these protons is reflected by the non-overlapping 3D surfaces, a fact which can be appreciated by the variable extent of the different color tones.

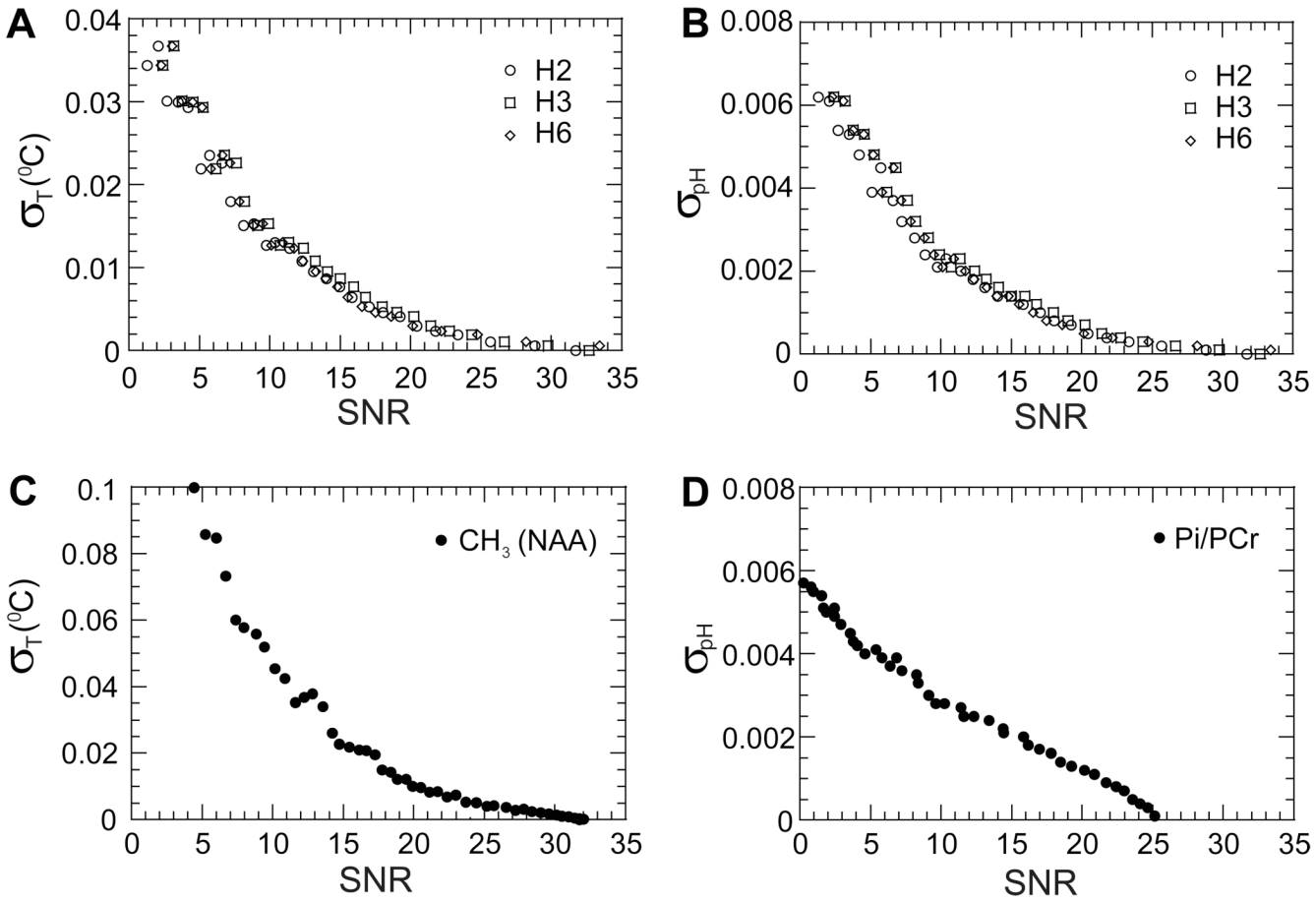

Figure 3.

Effect of spectral SNR on temperature and pH determination. Dependencies of temperature (A) and pH (B) standard deviations using the H2, H3 and H6 proton chemical shifts of $TmDOTP^{5-}$. For a typical *in vivo* SNR value of ~15, the standard deviations were 0.008 °C for temperature and 0.0013 for pH. The effect of SNR on temperature and pH accuracies was compared with the NAA-water method by ^{1}H MRS for temperature (C) and Pi-PCr method by ^{31}P MRS for pH (D). Under similar *in vivo* conditions, the SNR values were ~8 and ~5, respectively, which corresponded to standard deviations of 0.06 °C for temperature and 0.004 for pH.

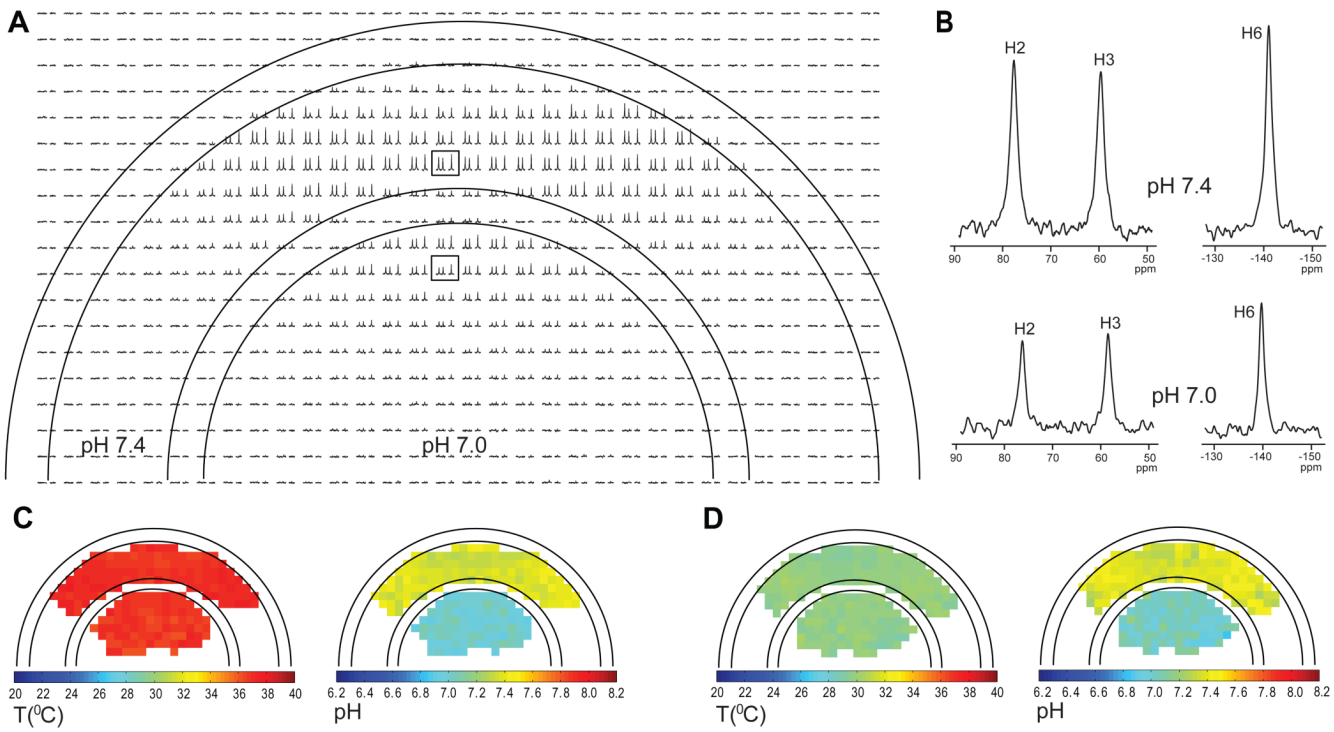

Figure 4.

Examples of temperature and pH maps of a two compartment phantom containing 4 mM $TmDOTP^{5-}$, 3 mM TSP and 1 mM Ca^{2+} in 10% D_2O at two different pH values (7.0 inner and 7.4 outer). (A) ^1H CSI of the phantom obtained in a 32×32 CSI experiment showing the resonances of H2, H3 and H6 protons. The bore temperature was initially maintained at 37.3 ±0.1 °C. The field of view used was 2.56×2.56 cm and the slice thickness was 4 mm, giving a voxel size of 0.8×0.8×4 mm^3. (B) Examples of ^1H spectra from two different voxels (boxed in A) one from the outer compartment at pH of 7.4 (upper spectrum) and the other from the inner compartment at pH of 7.0 (lower spectrum). Temperature and pH maps of the phantom at bore temperatures of 37.3±0.1 °C (C) and 30.1±0.1 °C (D).

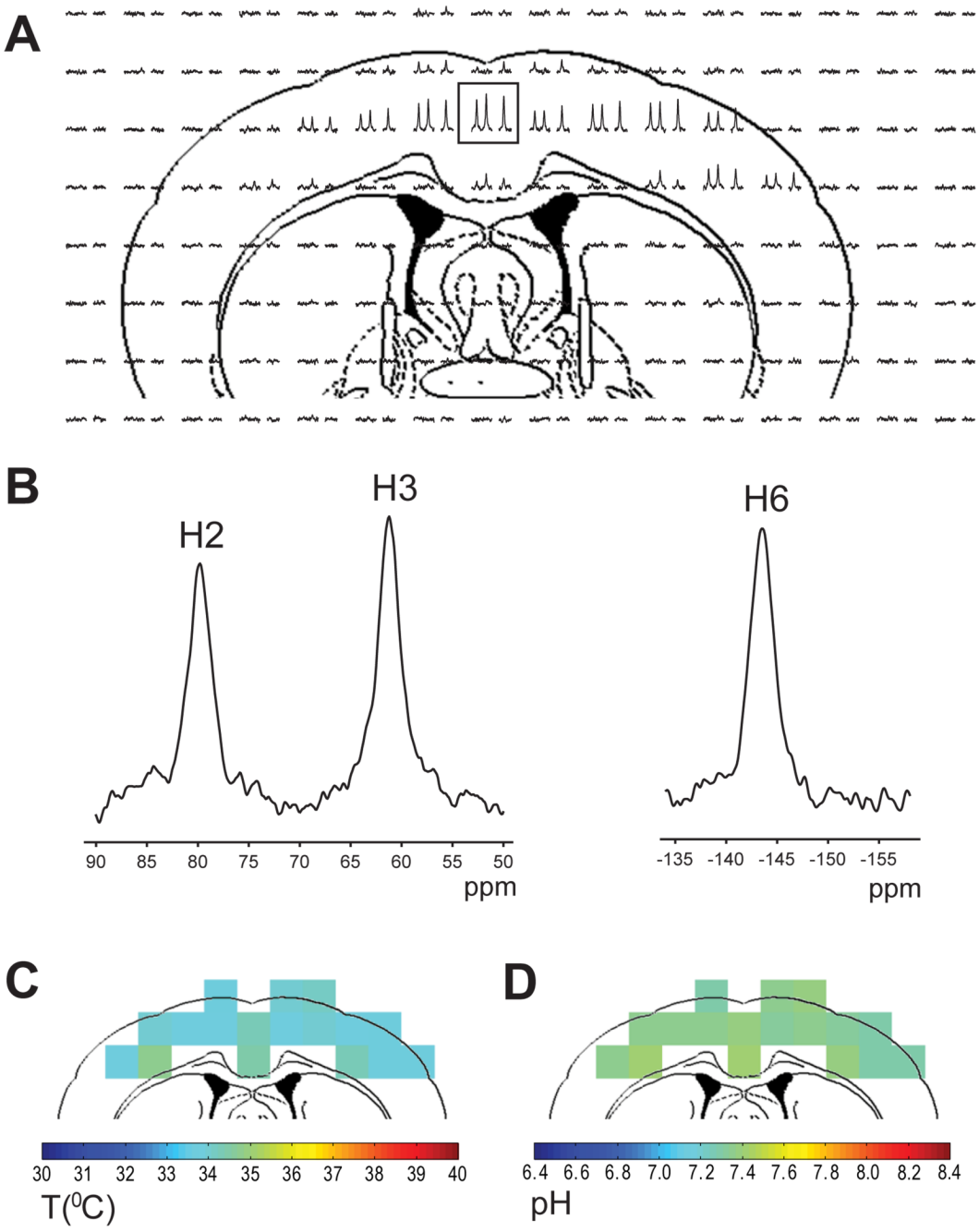

Figure 5.

Example of temperature and pH maps of rat brain. (A) ^{1}H CSI of rat brain after $TmDOTP^{5-}$ infusion. The signal intensity is much higher in the cortical area mainly due to RF inhomogeneity of the surface coil. (B) Example of ^{1}H spectra from a 1.6×1.6×4 mm^3 voxel (boxed in A) showing the H2, H3 and H6 proton resonances. (C) Temperature and (D) pH maps of rat brain.

Table 1

Longitudinal (T_1) and transverse (T_2) relaxation times for H1, H2, H3 and H6 protons of $TmDOTP^{5-}$ at 11.7T (temperature 35 °C, pH 7.4).

Proton	T_1 (ms)	T_2 (ms)
H1	0.40 ± 0.02	0.32 ± 0.03
H2	0.85 ± 0.03	0.47 ± 0.03
H3	0.88 ± 0.02	0.51 ± 0.04
H6	1.6 ± 0.1	0.73 ± 0.06

Table 2

Measured $TmDOTP^{5-}$ concentrations *in vivo*

Compartment	Fraction	$[TmDOTP^{5-}]$ (mM)
Blood	13 %	5.7 ± 0.3
Extracellular space	87 %	3.75 ± 0.12
Total	100 %	4.0 ± 0.1

Table 3

The coefficients $a_i^{[x,y]}$ for temperature determination using chemical shifts of two $TmDOTP^{5-}$ protons, x and y, for an *in vitro* sample (4 mM $TmDOTP^{5-}$, 1 mM Ca^{2+}; 10% D_2O). The coefficients were calculated from linear least-squares fits of temperature as function of chemical shifts according to eq. [5].

δ_x	δ_y	a_1	a_2	a_3	a_4	a_5	a_6
H2	H6	326.667	8.45179	7.68409	−0.0576860	0.0137429	−0.0193380
H3	H6	305.664	5.24485	4.94409	−0.1899355	−0.0193254	−0.1397433
H2	H3	176.503	52.60730	−70.54896	−16.2642940	−26.0607580	41.1884170

Table 4

The coefficients $b_i^{[x,y]}$ for pH determination using chemical shifts of two $TmDOTP^{5-}$ protons, x and y, for an *in vitro* sample (4 mM $TmDOTP^{5-}$, 1 mM Ca^{2+}, 10% D_2O). The coefficients were calculated from linear least-squares fits of pH as function of chemical shifts according to eq. [6].

δ_x	δ_y	b_1	b_2	b_3	b_4	b_5	b_6
H2	H6	8.085	1.42126	0.77861	−0.0084096	0.0007837	−0.0030817
H3	H6	2.261	0.59475	0.16352	−0.0391725	−0.0072995	−0.0329490
H2	H3	−15.069	10.63741	−13.05446	−2.3389974	−3.6943872	5.8774425